ACS OMEGA

Open Access

http://pubs.acs.org/journal/acsodf

Article

Effect of Nitrogen Introduction during (10$\bar{1}$0) ZnO Plasma-Assisted Molecular Beam Epitaxy on the Film Properties

Xiaodan Wang, Hua Zhou,* Regan G. Wilks, Tzung-En Hsieh, Wanli Yang, Yufeng Zhang, Huahan Zhan, Lihui Bai, Jin-Cheng Zheng, Marcus Bär,* Junyong Kang, and Hui-Qiong Wang*

Cite This: *ACS Omega* 2025, 10, 39639−39648

Read Online

ACCESS | Metrics & More | Article Recommendations | Supporting Information

ABSTRACT: Nitrogen doping is a commonly employed and effective strategy to achieve p-type ZnO films. A detailed understanding of the ZnO film growth behavior resulting in epitaxy is essential for elucidating the doping mechanism. In this study, ZnO films are grown on nonpolar (10$\bar{1}$0) ZnO substrates using plasma-assisted molecular-beam epitaxy (PA-MBE). Introducing nitrogen during PA-MBE growth is expected to lead to the incorporation of N, thus affecting the film properties. Growth kinetics, surface morphology, and chemical structure of the films are thus investigated through *in situ* reflection high-energy electron diffraction, *in-system* scanning tunneling microscopy, and *ex situ* synchrotron-based X-ray absorption spectroscopy. Well-ordered "stripe-like" structures are observed on the surface of the N-free ZnO films that evolve into "corn-like" nanostructures upon nitrogen addition and further transform into a "particle-like" morphology as the N_2/O_2 partial pressure ratio increases. Several nitrogen species, including N_2, NO, NO_2, and N_2O, are expected to exist during the growth process, with NO and NO_2 molecules suggested to predominantly adsorb onto (10$\bar{1}$0) ZnO surfaces, where N−Zn bonds are likely to form. A pathway for this chemical structural change is proposed. This work aims to explore whether the supply of nitrogen during PA-MBE growth results in the incorporation of nitrogen into the ZnO lattice and whether this can be considered a doping mechanism. Hence, this work might contribute to a better understanding of nitrogen incorporation, potentially realizing (and deliberately optimizing the) p-type doping of ZnO films.

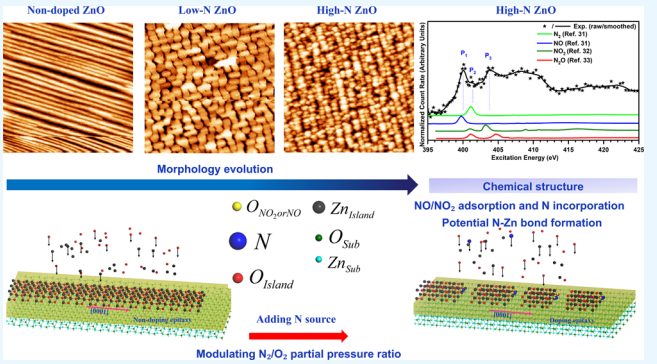

1. INTRODUCTION

Over the past few decades, zinc oxide (ZnO) has been regarded as a promising material to fabricate ultraviolet (UV) light emitters because of its large exciton binding energy of 60 meV and wide direct band gap of 3.37 eV at room temperature.[1] Reliably obtaining reproducible p-type-doped ZnO films is a prerequisite for realizing these kinds of devices, but it remains a significant challenge. To address this issue, strategies for p-type doping of ZnO are mainly classified into three types: (1) replacing Zn in the ZnO lattice with group IA elements; (2) substituting O sites in the ZnO lattice with group VA elements; and (3) employing a codoping approach involving both group IA and group VA elements.[2] The radius of group IA elements is often smaller than that of the Zn atom, making interstitial-site defects inevitable during film preparation, which easily leads to compensation of the generated holes. In the codoping method, the growth process and mechanisms of doping are often quite complex. Therefore, achieving reproducible p-type ZnO remains challenging, although recent studies have demonstrated some progress through carefully designed doping strategies.[3] The second strategy has been applied by many groups introducing VA elements such as N, P, As, and Sb.[4−7] Among these elements, nitrogen (N) stands out as one of the most promising candidates for p-type doping, not only because of its similar atomic radius but also due to its valence 2p energy levels and electronegativity, which are the closest to those of oxygen (O), especially compared to other group V dopants, and thereby is anticipated to substitute O (Nitrogen on a O site - N_O) as an acceptor.[8] While hybrid functional calculations reveal that N_O in N-doped ZnO possesses a high ionization energy of 1.3 eV,[9] suggesting that the observed p-type conductivity[4,10] in the compound may not be solely due to N_O, but more likely involves other N-containing complexes. Calculations suggest that N-related defect complexes, like N_O combined with a Zn vacancy (N_O-V_{Zn}), act as shallow acceptors and that p-type conductivity can be achieved through the formation of N_{Zn}-V_O,

Received: March 31, 2025
Revised: June 7, 2025
Accepted: June 11, 2025
Published: July 5, 2025

which then transforms into N_O-V_{Zn}-derived defect complexes.[11] This suggests that the behavior of N in ZnO is quite complex. As N has a different number of valence electrons than the Zn and O atoms in the host lattice, when nitrogen is incorporated into ZnO films, it also inevitably alters the surface morphology. A previous study has reported such morphology changes induced by N incorporation, primarily focusing on polar ZnO surfaces, and also demonstrated that *in-system* scanning tunneling microscopy (STM) is an effective technique for providing high-resolution observations to elucidate the mechanisms behind these N-induced changes.[12]

The polarity has a crucial impact on the optical and electrical properties of ZnO films.[13−15] ZnO epitaxial films and their heterostructures are typically grown along the *c*-axis (⟨0001⟩ direction), resulting in spontaneous polarization due to alternating zinc and oxygen ion layers, which lack inversion symmetry. Additionally, piezoelectric polarization arises from lattice mismatch-induced strain in ZnO-based heteroepitaxial structures. Together, these polarization effects create strong internal electric fields, which negatively impact device performance. These fields separate electron and hole wave functions, reducing the internal quantum efficiency of optoelectronic devices like light-emitting diodes (LEDs) and laser diodes (LDs).[16] In contrast, ZnO films epitaxially grown on nonpolar planes (a-plane or m-plane), whose surfaces are parallel to the *c*-axis and possess equal numbers of zinc and oxygen atoms, effectively eliminate the polarization effects seen in *c*-axis growth. This makes them highly promising for improving the performance of ZnO-based devices.[17] Nonpolar ZnO thin films and heterostructures have garnered significant attention.[18,19] Initially, nonpolar ZnO heterostructures were grown on sapphire substrates, resulting in high defect densities that limited luminescence efficiency, but this was later improved by using nonpolar ZnO substrates, which enabled higher-quality quantum well structures.[20,21] So far, studies on nitrogen doping in the homoepitaxial growth of nonpolar ZnO have not resulted in reliable p-type doping, despite the effective incorporation of nitrogen.[22,23] This suggests that as with polar ZnO, the mechanisms underlying nitrogen doping in nonpolar ZnO are quite complex. Nitrogen doping during the epitaxial process of nonpolar ZnO likely influences the growth behavior and morphology, as noted in the case of polar ZnO. These changes may, in turn, be interpreted as an indication that nitrogen indeed is incorporated as a dopant, which may potentially provide insights into the doping mechanisms. Our research group has previously conducted extensive research on the electronic structure of nonpolar ZnO and found that nitrogen incorporation induces significant variations in the electronic structure.[24] However, studies on the atomic-level surface morphology and growth mode of nonpolar N-doped ZnO remain limited.

In this work, $(10\bar{1}0)$ ZnO films were grown by plasma-assisted molecular beam epitaxy (PA-MBE). The growth mode and atomic-level surface morphology of the films were characterized by *in situ* reflection high-energy electron diffraction (RHEED) and *in-system* scanning tunneling microscopy (STM). In undoped ZnO, a stable $(10\bar{1}0)$ surface, characterized by stripe patterns parallel to the *c*-axis with step-edge features, was successfully obtained. Upon the introduction of N during ZnO growth, changes in the atomic step structure and surface topology were observed and compared with those of the N-free film. In addition, the effects of increasing nitrogen levels on the growth mode and surface structure were also investigated. The chemical environment of the nitrogen present in the sample was tentatively characterized using synchrotron-based X-ray absorption spectroscopy (XAS), indeed suggesting an incorporation of (some) nitrogen into the ZnO lattice. This study investigates the growth behavior and morphological changes induced by nitrogen introduction in nonpolar ZnO films with the aim of exploring potential nitrogen doping behaviors. It also seeks to advance the development of N-incorporated p-type ZnO and its potential applications in optoelectronic and semiconductor devices.

2. EXPERIMENTAL METHODS

2.1. Sample Preparation. Single-crystal $(10\bar{1}0)$ ZnO substrates were used for the growth of ZnO films. The sample preparation involved five main steps: substrate cleaning, substrate annealing, buffer layer deposition, buffer layer annealing, and film growth. First, the substrates underwent ultrasonic cleaning with acetone, ethanol, and deionized water before being transferred to an MBE system. Next, upon transfer to the growth chamber, the substrates were annealed at 300 °C in an O_2 atmosphere at a pressure of 5×10^{-5} mbar for 1 h, with O_2 plasma (99.999% purity, generating atomic oxygen species, purchased from Linde Gas Co., Ltd., Xiamen, China) activated at a power of 250 W. This treatment aims to clean the substrate surface, improve its structure, and optimize its chemical state for better film growth. Following this treatment, a homoepitaxial deposition of a ZnO buffer layer was carried out at 350 °C for 10 min, using a solid Zn source (99.9999% purity) and an O_2 plasma source. During the deposition of ZnO buffer layer, Zn was supplied by evaporating elemental Zn from a Knudsen cell, while oxygen was provided in the form of active oxygen radicals from an RF radical cell using a power of 250 W, maintaining the oxygen partial pressure at 5×10^{-5} mbar. The purpose of this step is to improve the crystalline quality, ensure minimal lattice mismatch, and provide a smoother surface for final film deposition. Subsequently, the samples underwent a second annealing step under an oxygen pressure of 5×10^{-5} mbar and a O_2 plasma source power of 250 W at 560 °C for 0.5 h. These conditions were used for substrate preparation and buffer layer deposition prior to the film growth of typical sets of ZnO samples. In the final step, one sample was grown using only the O_2 plasma and a Zn source, with an oxygen partial pressure of 1×10^{-5} mbar and plasma power of 250 W; designated as nondoped ZnO. For the other two samples, N_2 was introduced during the growth process. Specifically, an N_2 plasma source (99.999% purity, generating atomic nitrogen species, purchased from Linde Gas Co., Ltd., Xiamen, China) with RF power was used alongside the O_2 source, with N_2/O_2 pressure ratios of 5:1 and 9:1, respectively, designated as ZnO with low N and high N content. The N_2 plasma power was set at 300 W, operating in parallel with the O_2 plasma, which was set at 250 W. For all samples, the growth time was 1.5 h, with a constant Zn beam flux from the Knudsen cell maintained at 360 °C. The substrate temperature was consistently held at 500 °C throughout the growth.

2.2. Sample Characterization. RHEED was employed to examine the surface structure of both the ZnO substrate prior to deposition and the ZnO films after deposition. RHEED offers the advantage of real-time, nondestructive monitoring during MBE. In the RHEED setup, a high-energy electron beam (with energy typically between 10 and 50 keV) is

https://doi.org/10.1021/acsomega.5c02932
ACS Omega 2025, 10, 39639−39648

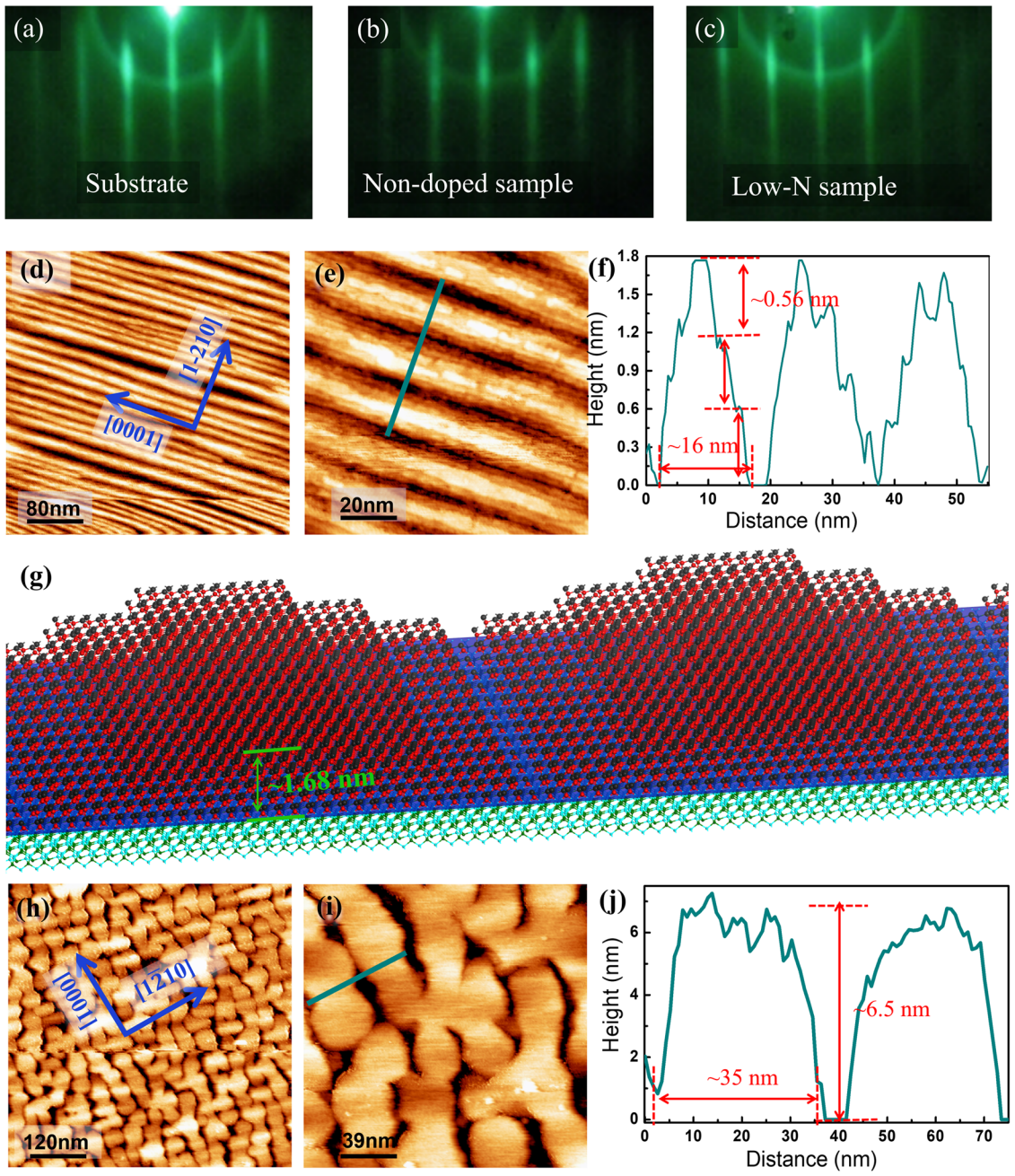

Figure 1. (a) RHEED patterns along the $\langle 11\bar{2}0\rangle$ direction from the $(10\bar{1}0)$ ZnO substrate; (b) RHEED patterns along the $\langle 11\bar{2}0\rangle$ direction from the nondoped sample; (c) RHEED patterns along the $\langle 11\bar{2}0\rangle$ direction from the low-N sample. (d) Large-scale STM image (400×400 nm^2) of the nondoped ZnO film; (e) small-scale STM image (100×100 nm^2) of the nondoped ZnO film; (f) profile plot along the line in (e); (g) three-dimensional atomic model of the nondoped ZnO film; (h) large-scale STM image (600×600 nm^2) of the low-N ZnO film; (i) small-scale STM image (190×190 nm^2) of the low-N ZnO film; (j) profile plot along the line in (i).

generated by an electron gun and directed toward the sample surface at a grazing incidence angle of approximately 1−3°. The electron beam's acceleration voltage, supplied by the UHV-MBE control power supply, is continuously adjustable within the range of 0−20 kV, while the beam current can be adjusted within the range of 0−2.0 A. In our setup, the acceleration voltage is set to 15 kV, and the filament current is adjusted to 1.5 A. Due to the grazing incidence and the weak inelastic scattering at this energy level, the primary interaction is elastic scattering, and the resulting diffraction pattern is projected onto a phosphor screen. The diffraction patterns, such as streaks or spots, provide real-time insights into the surface morphology and crystal structure of the sample. When the surface is well ordered, the RHEED pattern appears sharp, often revealing Kikuchi lines. Conversely, as the surface becomes rougher, the streaks in the diffraction pattern transition into broader diffraction spots.

The *in-system* STM measurements were conducted using an ultrahigh-vacuum (UHV) system equipped with a room-temperature STM (Omicron STM-1), operating at a base pressure of 2×10^{-10} mbar to ensure stable conditions for high-resolution surface characterization. After the growth of all samples was completed, they were immediately transferred under ultrahigh vacuum to the STM chamber without

https://doi.org/10.1021/acsomega.5c02932
ACS Omega 2025, 10, 39639−39648

exposure to air, where STM measurements were conducted. All images were acquired at room temperature using constant current mode, providing critical insights into the growth behavior and surface characteristics of the ZnO samples.

XAS measurements of the ZnO sample with high N content at the N K-edge were performed at Beamline 8.0.1 of the Advanced Light Source (ALS), Lawrence Berkeley National Laboratory, using the SALSA endstation.[25] XAS spectra were recorded in bulk-sensitive partial fluorescence yield (PFY) mode utilizing SALSA's high-transmission X-ray spectrometer[26] recording the N K-edge emission. The XAS data was normalized by the incident photon flux measured using a clean gold mesh placed upstream. The photon energy was calibrated by measuring the N K-edge XAS spectra of N_2 gas as a standard. Prior to the measurement, the sample was briefly exposed to ambient conditions during the sample mounting process.

3. RESULTS AND DISCUSSION

3.1. Nitrogen-Induced Surface Morphology Transformation in (10$\bar{1}$0) ZnO Films. Figure 1a–c displays the *in situ* RHEED patterns captured along the ⟨11$\bar{2}$0⟩ azimuth of the single-crystalline (10$\bar{1}$0) ZnO substrate, nondoped ZnO film, and the low-N ZnO film, respectively. The bright streaks in Figure 1a indicate a flat surface on the ZnO substrate after annealing. After 1.5 h of ZnO film growth (corresponding to a thickness of about 150 nm), the RHEED patterns for both the nondoped and low-N films remain streaky with little change, as seen in Figure 1b,c, closely resembling the pattern of the substrate. This suggests that the film surfaces for these samples remain relatively flat, further indicating the high quality of the films grown homoepitaxially on the (10$\bar{1}$0) substrate.

To explore the impact of nitrogen incorporation on the growth behavior and morphology, we investigate the samples by *in-system* STM, i.e., sample preparation and characterization were done in one interconnected vacuum system. Figure 1d,e shows STM images of the nondoped sample at low(er) and high(er) magnification. The nondoped film displays stripes along the *c*-axis, very similar to horizontally and uniformly arranged ZnO nanowires. This observation suggests that ZnO grows much faster along the *c*-axis than along other directions, which can be attributed to two factors: (I) the surface energy of the polar plane is larger than those of other surfaces,[27−29] making adatoms easier to form O−Zn bonds on the (0001) surface than on the other surfaces; (II) the diffusion length (barrier) along the ⟨0001⟩ direction is larger (smaller) than that along ⟨1$\bar{2}$10⟩ direction.[30,31] The profile line in Figure 1f along the ⟨1$\bar{2}$10⟩ azimuth, indicated as a deep green line in Figure 1e, reveals that the width of the bright stripes is about 16 nm, which equals to about 50 times the lattice constant along ⟨1$\bar{2}$10⟩, and the depth of the stripes is about 1.68 nm, i.e., approximately 3 times the vicinal step height (∼0.56 nm), as labeled by the red double arrows in Figure 1f. This result suggests that the vicinal step height corresponds to the height of a single atomic layer ($\sqrt{3}a_{ZnO} \sim 0.56$ nm). Additionally, the observed maximum mean peak-to-valley height (∼1.68 nm) suggests minimal surface roughness, in agreement with the RHEED results. With the edges of the stripes aligned along the *c*-axis and exhibiting atomic steps, as shown in Figure 1f, the growth is likely occurring in a step-flow mode. This step-flow growth mode has also been observed in O-polar ZnO to stabilize the surface.[12] In studies of nonpolar ZnO, such surface morphology with anisotropic stripe patterns has been extensively observed,[22,32] but atomic-level step edges have rarely been reported. The observed surface structure, characterized by a horizontally and uniformly arranged small nanowire-type topography and low surface roughness, suggests that achieving high-quality films is more feasible along the [10$\bar{1}$0] orientation compared to the [0001] orientation, as indicated in Figure 1d. Based on the above analysis, corresponding 3D atomic models for the observed surface structure of the horizontally arrayed wire-type topography can be constructed, as illustrated in Figure 1g. Notably, for the low-N ZnO film, the parallel stripe arrays disintegrate and develop pronounced wrinkling, transforming into a ″corn-like″ nanostructure with staggered patterns, as shown in Figure 1h,i. Additionally, the width and depth of the stripes increase, measuring approximately 35 nm in width and 6.5 nm in depth, as shown by the profile line in Figure 1j.

These observations indicate that the surface morphology undergoes a clear topological transformation with nitrogen incorporation. For nondoped ZnO films, the surface is dominated by parallel stripes along the *c*-axis, reflecting an anisotropic growth mode. As nitrogen is introduced, these stripes interconnect and gradually merge for the low-N ZnO sample, indicating a shift in surface topology, likely due to the disruption of anisotropic adatom growth. It should also be noted that the edges of the merged stripes no longer exhibit atomic step characteristics, as shown in Figure 1j. In summary, the *in-system* STM images indicate that nitrogen introduction significantly impacts the growth dynamics and topological surface morphology of (10$\bar{1}$0) ZnO films.

Underneath these nitrogen-induced changes must lie important mechanisms related to the behavior of N incorporation. In the nonpolar case, the changes in atomic step kinetics and surface morphology have been demonstrated to result from the incorporation of nitrogen.[12] That study confirms the successful incorporation of N into the ZnO lattice and hence can be considered to be indicative of N doping. Furthermore, it has been suggested that this doping primarily occurs at step edges and provides a path for producing V_{Zn}−N_O defect complexes, which are considered shallow acceptors.[36] Turning to our case, although we lack direct evidence for the incorporation of nitrogen into the ZnO lattice, the significant changes in atomic step kinetics and topological morphology strongly suggest the interaction of nitrogen with the Zn and the O atoms. If nitrogen (or related species) was introduced without interaction with the ZnO lattice or solely adsorbed onto the surface during the ZnO PA-MBE deposition process, the impact on growth modes and surface topology would be minimal and could not explain the observed morphological changes. The stripe interconnection and disruption of anisotropic growth rates indicate that nitrogen likely interacts chemically with the lattice, altering the surface energy and adatom mobility. Thus, nitrogen incorporation or strong surface interaction is likely responsible for these transformations.

3.2. Effect of Increased Nitrogen Level on Growth Mode of (10$\bar{1}$0) ZnO Films and Nitrogen Chemical Structure. By repeating the growth procedure, another sample was fabricated with the N_2 to O_2 partial pressure ratio increased from 5:1 to 9:1, which is referred to as the high-N ZnO sample. Building on the significant changes induced by nitrogen introduction with the growth kinetics and topological morphology details already described, we proceeded with attempts to further increase the nitrogen levels in the ZnO

https://doi.org/10.1021/acsomega.5c02932
ACS Omega 2025, 10, 39639−39648

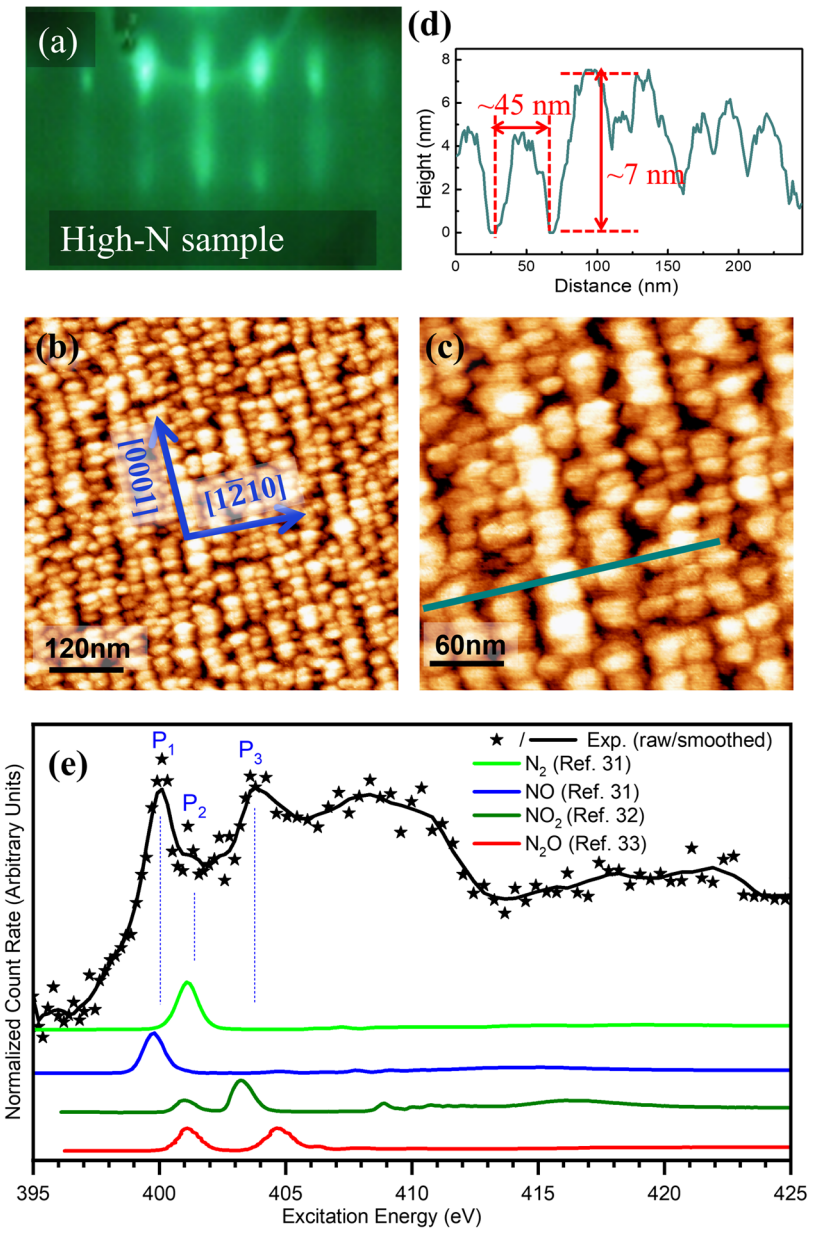

Figure 2. (a) RHEED patterns along the $\langle 11\bar{2}0 \rangle$ direction from the high-N ZnO sample. (b) Large-scale (600×600 nm^2) STM images of high-N ZnO film; (c) small-scale (300×300 nm^2) STM images of high-N ZnO film; (d) profile plot along the line in (c). (e) Experimental N K-edge X-ray absorption spectrum for the high-N ZnO sample, compared with reference spectra for N_2 and NO obtained from the gas phase core excitation database[33] and additional reference spectra for NO_2[34] and N_2O[35] reported in the literature.

sample and explore the corresponding impact. We observed that the changes become more pronounced as the N_2/O_2 ratio increases. The RHEED pattern transitions from streaky to spotty, as shown in Figure 2a for the high-N sample compared with Figure 1a,b, indicating an increase in surface roughness. This indicates that the growth mode has transitioned from 2D to 3D. In addition, the topography changes again, as demonstrated by the *in-system* STM images in Figure 2b,c. In contrast to the previous trends seen in Figure 1d−j, where the stripe patterns tended to merge, the morphology of the high-N ZnO sample, as shown in Figure 2b,c, reveals a disruption of the stripe continuity along the *c*-axis. The stripes no longer merge but instead become increasingly discontinuous. From a topological morphology perspective, this suggests a breakdown of the ordered pattern, resulting in a more fragmented surface structure. This observation suggests that an increase in the N level further roughens the film surface and transitions the growth mode from 2D to 3D, which aligns with the RHEED pattern observations. This change could be attributed to nitrogen doping, which might introduce additional surface stress and disrupt the atomic arrangement along the *c*-axis. As doping may introduce stress or affect atomic mobility, further promoting three-dimensional island growth, we infer that the increased partial pressure ratio of N_2 to O_2 in our case may raise the doping levels and this further supports the inference that nitrogen is indeed incorporated into the lattice. Notably, the width and depth of the stripes increase approximately to about 45 and 7 nm, respectively, as depicted by the profile in Figure 1j. Interestingly, these values are quite close to those of the low-N samples (35 and 6.5 nm), yet the RHEED pattern shows a significant difference (Figures 1c and 2a). While the stripe dimensions remain similar, RHEED's

https://doi.org/10.1021/acsomega.5c02932
ACS Omega 2025, 10, 39639−39648

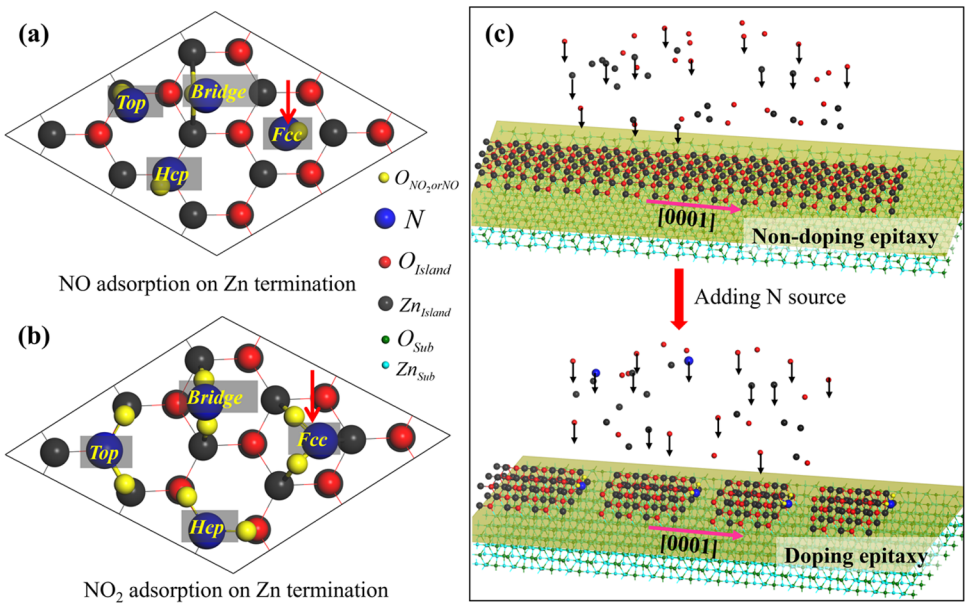

Figure 3. Atomic model of N source adsorptions and schematics of N source reactions. (a, b) Atomic models of three adsorption sites with the lowest adsorption energy for NO and NO_2 on the Zn termination; (c) schematics for the change of the morphology induced by selected adsorption and reaction of the N source during the epitaxy.

sensitivity to surface morphology reveals a shift from 2D growth mode in the low-N case to 3D island growth mode in the high-N sample. We think that the following reasons may account for these observations: In the low-N ZnO sample, the surface grows in a 2D mode, with stripes starting to merge, maintaining a relatively flat surface and producing a smoother RHEED pattern. In contrast, the high-N ZnO sample, despite having similar stripe dimensions, undergoes a transition to 3D growth, resulting in a grainier surface and more electron beam scattering. This shift in growth mode and increased surface roughness likely account for the significant differences in the RHEED patterns, even with comparable dimensions. This transition in growth mode, accompanied by increased surface roughness, is likely responsible for the pronounced discrepancies observed in the RHEED patterns, despite the comparable stripe dimensions.

In order to gather further information about the chemical structure of nitrogen incorporated into ZnO, we performed XAS experiments on the high-N ZnO sample next. The measurements focused on the N K-edge, where we successfully obtained a clear signal, confirming nitrogen to be present in the sample, as shown in Figure 2e. The black star symbols and the black solid curve represent the normalized experimental N K-edge XAS data before and after smoothing (smoothing was performed in Origin using a 5-point weighted-adjacent-average). We note that the XAS spectrum is dominated by two strong peaks at approximately 400.1 eV (P_1) and 403.9 eV (P_3) and one shoulder peak at the high photon energy side of P1 at approximately 400.8 eV, labeled P_2. Previous studies suggest that during nitrogen-ion bombardment of ZnO, the process (by breaking Zn−O bonds) may result in the formation of Zn−N, −O, or Zn−N−O bonds. In our experiment, N_2 and O_2 are dissociated by the plasma into (reactive) nitrogen and oxygen atoms. During the growth process, these reactive species may similarly interact with surface zinc atoms, potentially forming N-related bonds, including N−N, Zn−N, N−O, or Zn−N−O bonds, as the plasma provides a high-energy environment, allowing for a diverse and complex combination of nitrogen and oxygen bonding with zinc. To attempt to identify and interpret the observed peaks, the N K-edge core excitation spectra of N_2 and NO[33] along with N K-edge XAS spectra of NO_2[34] and N_2O,[35] are presented in Figure 2e for direct comparison. Note that there could easily be a negative or positive shift in the photon energy scale between the individual data sets. Considering this, it is apparent that our spectral features P_1 and P_2 as well as P_3 could to some extent indeed be explained by the presence of N_2, NO, NO_2, and N_2O (or a combination thereof) as well as by the presence of NO and/or NO_2, respectively. It is unclear whether these gases have indeed been incorporated into the ZnO film during the PA-MBE process or whether the corresponding N−N or N_x−O_y bonds have been formed in the film. However, it is clear that the spectral region below 400 eV and above 405 eV, i.e., the photon energy regime where spectral features of Zn−N bonds and N−O bonds,[37] respectively, are expected, cannot be explained by the spectral signature of N_2, NO, NO_2, and N_2O (or a superposition thereof), which might be interpreted as the incorporation of nitrogen into the ZnO lattice, which aligns with the interpretation of the STM images. While the present study does not explore the potential p-type conductivity of the synthesized N-doped ZnO, this finding might also point at the possibility of achieving p-type doping in such materials.

3.3. Possible Mechanisms of Nitrogen Incorporation in (10$\bar{1}$0) ZnO Films. To explore the mechanisms underlying these observations, we consider the adsorption behavior of nitrogen species on ZnO films during growth. As mentioned above, nitrogen is likely to reach the surface of the ZnO film in various molecular forms, which subsequently interact with the ZnO lattice, facilitating further chemical reactions. Considering that previous theoretical studies have demonstrated that, among various nitrogen-related dopant gases used during ZnO growth, only NO and NO_2 are favorable from a chemical potential perspective for supplying soluble, isolated nitrogen that can readily be incorporated into the ZnO lattice,[38,39] and given that N_2 exhibits exceptional stability, with a bond

https://doi.org/10.1021/acsomega.5c02932
ACS Omega 2025, 10, 39639−39648

dissociation energy of 78,691.09 cm^{-1},[40] which likely results in minimal reactivity with O or Zn atoms, we hypothesize that the most prominent nitrogen-containing species adsorbed on the $(10\bar{1}0)$ ZnO sample are NO and NO_2. We specifically focus on previous theoretical studies examining the adsorption energies of these two species on ZnO surfaces. A literature survey of previous density functional theory (DFT) studies revealed that the lowest adsorption energies of NO and NO_2 on various ZnO surfaces differ significantly. The results consistently show that the adsorption energies on polar surfaces are markedly lower than those on nonpolar surfaces, indicating a stronger interaction on the polar facets. This trend is reported across multiple studies, as summarized in Table S1. These results indicate that the chemical states of nitrogen are more reactive toward Zn or O adatoms on the c-plane surface, which is consistent with findings reported in a previous study.[24] Kato et al. and Nakahara et al. have experimentally shown that Zn termination enhances the quality of ZnO films and facilitates N-doping.[10,41] Therefore, we here focus specifically on the interactions between N species and a Zn-terminated ZnO surface. Figure 3a,b illustrates the atomic models of NO and NO_2 adsorbing on the Zn-terminated ZnO and gives the adsorption energy at the different sites. Previous theoretical studies[42,43] have investigated the most stable adsorption sites for NO and NO_2 on ZnO surfaces, considering several typical surface configurations. The results indicate that the lowest energy adsorption sites for both NO and NO_2 are located at the fcc sites, as indicated by the red arrows in Figure 3a,b, respectively. Based on the analysis above, it can be inferred that NO and NO_2 prefer to adsorb at the fcc sites of the (0001) ZnO surface even during the epitaxial growth of a $[10\bar{1}0]$ oriented film. When NO or NO_2 adsorb at the fcc sites, these sites often become nucleation points for new island formation due to their large negative adsorption energies (about −1.48 eV for NO[42] and −3.14 eV for NO_2[43]). In this way, the significant differences observed in both growth behavior and topological morphology due to the introduction of N can be understood from two perspectives: the growth rate and the nucleation process. First, NO or NO_2 may saturate the dangling bonds and neutralize the excess electrons caused by the built-in field along the *c*-axis, leading to a reduction in the surface energy on the c-plane. As a result, the preferential growth along the *c*-axis, which typically promotes the formation of aligned wire-like morphologies, becomes significantly diminished. At the same time, lateral growth along the $\langle 1\bar{2}10\rangle$ azimuth becomes more pronounced due to the reduced growth along the *c*-axis, leading to an increase in the width of the parallelly arrayed stripes, as shown in Figure 1i,j. Second, the newly nucleated islands generate numerous wrinkles and disrupt the continuity of the arrayed stripes, which may actually contribute to the changes in topological morphology, as observed in the in situ STM images in Figure 1h,i. The above analysis suggests that during growth without N, nucleation in the $[10\bar{1}0]$ orientation tends to form elongated chain structures with heights of approximately 1−3 unit cells, as shown in the atomic model in Figure 1g. When N is introduced, NO and NO_2 may predominantly adsorb at the fcc sites, promoting the nucleation of new islands and disrupting the parallel long chains as schematically illustrated in Figure 3c. At a higher N_2/O_2 ratio, the nucleated islands likely further fragment the arrayed stripes, making them even shorter, as seen in Figure 2b,c. Note that in the above analysis, we do not discuss N atoms separately, as the N radicals produced by plasma are highly reactive and unstable, quickly reacting with O or O_2 to form nitrogen oxides.

While the adsorption of NO and NO_2 provides a plausible explanation for the observed morphological and kinetic changes, it is important to distinguish between surface adsorption and lattice incorporation. The former refers to nitrogen species interacting with the outermost atomic layers and influencing surface processes without entering the crystal lattice,[44] whereas the latter involves nitrogen atoms being incorporated into the crystal structure, for example by substituting for oxygen, a process that has been theoretically shown to generate shallow acceptor states and enable p-type conductivity.[45] Our current analysis focuses on adsorption-mediated surface interactions during growth, which we believe contribute to nitrogen incorporation. A conclusive determination of nitrogen incorporation requires further chemical, electrical, and structural characterization.

Combining the RHEED patterns, STM images, XAS results, and adsorption behavior analysis, it is reasonable to expect that the introduction of N during the growth of ZnO indeed leads to the interaction of nitrogen with the ZnO lattice, indicating a possibility for successful nitrogen doping. We propose a potential pathway for N incorporation in ZnO via NO and NO_2 molecules adsorbing onto $(10\bar{1}0)$ ZnO surfaces, serving as nitrogen source during ZnO growth and leading to nitrogen incorporation through the formation of N-related defects.

4. CONCLUSIONS

In conclusion, we have explored the homoepitaxial growth of ZnO thin films under varying N_2/O_2 pressure ratios (including a N-free case) using the PA-MBE method, aiming to understand the effects of nitrogen introduction and investigate potential doping behaviors. RHEED patterns reveal a transition in growth mode from 2D to 3D upon nitrogen introduction. *In-system* STM imaging reveals significant changes in the morphology of ZnO films, which were initially characterized by parallel "stripe-like" structures in the undoped case, evolving into "corn-like" nanostructures upon nitrogen introduction, and further transforming into a "particle-like" morphology as the N_2/O_2 partial pressure ratio increased. Synchrotron-based N K-edge XAS experiments indicate interactions between nitrogen species and the ZnO lattice. It is proposed that NO and NO_2 molecules adsorb onto $(10\bar{1}0)$ ZnO surfaces, potentially serving as nitrogen sources. This adsorption may lead to the formation of N-related defects, facilitating nitrogen incorporation and the interaction of nitrogen with the ZnO lattice, which contribute to the observed changes in the morphology and growth behavior. These findings provide insights into how nitrogen incorporation alters the surface morphology and growth behavior of the ZnO films. Such modifications are likely to impact surface quality and interface properties, which are essential for improving carrier dynamics in ZnO-based photoelectronic devices.

■ ASSOCIATED CONTENT

Data Availability Statement

All data supporting the findings of this study are included in the manuscript and Supporting Information.

Supporting Information

The Supporting Information is available free of charge at https://pubs.acs.org/doi/10.1021/acsomega.5c02932.

https://doi.org/10.1021/acsomega.5c02932
ACS Omega 2025, 10, 39639−39648

Reported NO and NO_2 adsorption energies on different ZnO surfaces and associated references (PDF)

AUTHOR INFORMATION

Corresponding Authors

Hua Zhou − *School of Physics, Shandong University, Jinan 250100, China*; Email: zhouhua2018@sdu.edu.cn

Marcus Bär − *Department of Interface Design, Helmholtz-Zentrum Berlin für Materialien und Energie GmbH (HZB), 12489 Berlin, Germany; Energy Materials In-situ Laboratory Berlin (EMIL), Helmholtz-Zentrum Berlin für Materialien und Energie GmbH (HZB), 12489 Berlin, Germany; Department of Chemistry and Pharmacy, Friedrich-Alexander-Universität Erlangen-Nürnberg (FAU), 91058 Erlangen, Germany; Department of X-ray Spectroscopy at Interfaces of Thin Films, Helmholtz Institute Erlangen-Nürnberg for Renewable Energy (HI ERN), 12489 Berlin, Germany;* orcid.org/0000-0001-8581-0691; Email: marcus.baer@helmholtz-berlin.de

Hui-Qiong Wang − *Engineering Research Center of Micro-nano Optoelectronic Materials and Devices, Ministry of Education, Fujian Key Laboratory of Semiconductor Materials and Applications, CI Center for OSED, and Department of Physics, Xiamen University, Xiamen 361005, China; Xiamen University Malaysia, Sepang 43900, Malaysia;* orcid.org/0000-0002-0495-3146; Email: hqwang@xmu.edu.cn

Authors

Xiaodan Wang − *Engineering Research Center of Micro-nano Optoelectronic Materials and Devices, Ministry of Education, Fujian Key Laboratory of Semiconductor Materials and Applications, CI Center for OSED, and Department of Physics, Xiamen University, Xiamen 361005, China; Department of Interface Design, Helmholtz-Zentrum Berlin für Materialien und Energie GmbH (HZB), 12489 Berlin, Germany*

Regan G. Wilks − *Department of Interface Design, Helmholtz-Zentrum Berlin für Materialien und Energie GmbH (HZB), 12489 Berlin, Germany; Energy Materials In-situ Laboratory Berlin (EMIL), Helmholtz-Zentrum Berlin für Materialien und Energie GmbH (HZB), 12489 Berlin, Germany;* orcid.org/0000-0001-5822-8399

Tzung-En Hsieh − *Department of Interface Design, Helmholtz-Zentrum Berlin für Materialien und Energie GmbH (HZB), 12489 Berlin, Germany;* orcid.org/0000-0003-1844-2635

Wanli Yang − *Advanced Light Source (ALS), Lawrence Berkeley National Laboratory, Berkeley, California 94720, United States;* orcid.org/0000-0003-0666-8063

Yufeng Zhang − *Engineering Research Center of Micro-nano Optoelectronic Materials and Devices, Ministry of Education, Fujian Key Laboratory of Semiconductor Materials and Applications, CI Center for OSED, and Department of Physics, Xiamen University, Xiamen 361005, China;* orcid.org/0000-0001-7956-7250

Huahan Zhan − *Engineering Research Center of Micro-nano Optoelectronic Materials and Devices, Ministry of Education, Fujian Key Laboratory of Semiconductor Materials and Applications, CI Center for OSED, and Department of Physics, Xiamen University, Xiamen 361005, China;* orcid.org/0000-0002-3370-9193

Lihui Bai − *School of Physics, Shandong University, Jinan 250100, China*

Jin-Cheng Zheng − *Engineering Research Center of Micro-nano Optoelectronic Materials and Devices, Ministry of Education, Fujian Key Laboratory of Semiconductor Materials and Applications, CI Center for OSED, and Department of Physics, Xiamen University, Xiamen 361005, China; Xiamen University Malaysia, Sepang 43900, Malaysia;* orcid.org/0000-0002-6292-3236

Junyong Kang − *Engineering Research Center of Micro-nano Optoelectronic Materials and Devices, Ministry of Education, Fujian Key Laboratory of Semiconductor Materials and Applications, CI Center for OSED, and Department of Physics, Xiamen University, Xiamen 361005, China*

Complete contact information is available at: https://pubs.acs.org/10.1021/acsomega.5c02932

Author Contributions

All authors were involved in the data analysis, interpretation, and manuscript preparation. All authors reviewed and approved the final version of the manuscript.

Notes

The authors declare no competing financial interest.

ACKNOWLEDGMENTS

This work was supported by the National Key Research and Development Program of China (Grant No. 2022YFB3605403) and the Sino-German (CSC-DAAD) Postdoc Scholarship Program (Grant No. 57678375).

REFERENCES

(1) Özgür, Ü.; Alivov, Y. I.; Liu, C.; Teke, A.; Reshchikov, M. A.; Dogan, S.; Avrutin, V.; Cho, S. J.; Morkoc, H. A comprehensive review of ZnO materials and devices. *J. Appl. Phys.* **2005**, *98*, No. 041301.

(2) Yang, R.; Wang, F.; Lu, J.; Lu, Y.; Lu, B.; Li, S.; Ye, Z. ZnO with P-Type Doping: Recent Approaches and Applications. *ACS Appl. Electron. Mater.* **2023**, *5* (8), 4014−4034.

(3) Zak, A. K.; Hashim, A. M. Optical Properties and Band-Gap Engineering of Group (I) Element-Doped ZnO Nanoparticles as P-Type Semiconductors. *Opt. Mater.* **2024**, *152*, No. 115434.

(4) Look, D. C.; Reynolds, D. C.; Litton, C. W.; Jones, R. L.; Eason, D. B.; Cantwell, G. Characterization of homoepitaxial p-type ZnO grown by molecular beam epitaxy. *Appl. Phys. Lett.* **2002**, *81*, 1830−1832.

(5) Wang, P.; Chen, N.; Yin, Z. G.; Yang, F.; Peng, C. T.; Dai, R. X.; Bai, Y. M. As-doped p-type ZnO films by sputtering and thermal diffusion process. *J. Appl. Phys.* **2006**, *100*, No. 043704.

(6) Kim, K. K.; Kim, H. S.; Hwang, D. K.; Lim, J.-H.; Park, S.-J. Realization of p-type ZnO thin films via phosphorus doping and thermal activation of the dopant. *Appl. Phys. Lett.* **2003**, *83*, 63−65.

(7) Liu, M.; Sha, S.; Xi, Z.; Tang, K.; Wan, P.; Kan, C.; Shi, D.; Jiang, M. Precise p-Type Doping of ZnO Microwires for Electrically-Pumped Homojunction Microlaser Diode. *J. Mater. Sci. Technol.* **2026**, *243*, 89.

(8) Harrison, W. A. *Elementary Electronic Structure*; World Scientific: Singapore, 1999.

(9) Lyons, J. L.; Janotti, A.; Van de Walle, C. G. Why nitrogen cannot lead to p-type conductivity in ZnO. *Appl. Phys. Lett.* **2009**, *95*, No. 252105.

(10) Kato, H.; Yamamuro, T.; Ogawa, A.; Kyotani, C.; Sano, M. Impact of Mixture Gas Plasma of N_2 and O_2 as the N Source on ZnO-Based Ultraviolet Light-Emitting Diodes Fabricated by Molecular Beam Epitaxy. *Appl. Phys. Express* **2011**, *4*, No. 091105.

(11) Liu, L.; Xu, J. L.; Wang, D. D.; Jiang, M. M.; Wang, S. P.; Li, B. H.; Zhang, Z. Z.; Zhao, D. X.; Shan, C.-X.; Yao, B.; Shen, D. Z. p-Type Conductivity in N-Doped ZnO: The Role of the N_{Zn}-V_O Complex. *Phys. Rev. Lett.* **2012**, *108*, No. 215501.
(12) Wang, H.; Zhan, H. H.; Zhou, Y. H.; Wu, Y. P.; Chen, X. H.; Wang, H. Q.; Kang, J. Y. Effects of nitrogen dopants on the atomic step kinetics and electronic structures of O-polar ZnO. *Nanoscale* **2016**, *8*, 4381−4386.
(13) Zhang, Y.; Du, G.; Zhu, H.; Hou, C.; Huang, K.; Yang, S. Comparisons of Structural and Optical Properties of ZnO Films Grown on (0001) Sapphire and (01$\bar{1}$2) Sapphire by Low-Pressure MOCVD. *Opt. Mater.* **2004**, *27* (3), 399−402.
(14) Zúñiga-Pérez, J.; Muñoz-Sanjosé, V.; Palacios-Lidón, E.; Colchero, J. Polarity Effects on ZnO Films Grown along the Nonpolar [11$\bar{2}$0] Direction. *Phys. Rev. Lett.* **2005**, *95* (22), No. 226105.
(15) Zhu, J. J.; Aaltonen, T.; Venkatachalapathy, V.; Galeckas, A.; Kuznetsov, A. Yu. Structural and Optical Properties of Polar and Non-Polar ZnO Films Grown by MOVPE. *J. Cryst. Growth* **2008**, *310* (23), 5020−5024.
(16) Wetzel, C.; Takeuchi, T.; Amano, H.; Akasaki, I. Quantized states in $Ga_{1-x}In_xN$/GaN heterostructures and the model of polarized homogeneous quantum wells. *Phys. Rev. B* **2000**, *62*, No. R13302.
(17) Chen, J. J.; Deng, X. R.; Deng, H. Progress in the growth and characterization of nonpolar ZnO films. *J. Mater. Sci.* **2013**, *48*, 532−542.
(18) Lautenschlaeger, S.; Eisermann, S.; N Hofmann, M.; Udo Roeme, U.; Pinnisch, M.; Laufer, A.; K Meyer, B.; Wenckstern, H. V.; Lajn, A.; Schmidt, F.; Grundmann, M.; Blaesing, J.; Krost, A. Morphological, structural and electrical investigations on non-polar a-plane ZnO epilayers. *J. Cryst. Growth* **2010**, *312*, 2078−2082.
(19) Gangil, S.; Nakamura, A.; Shimomura, M.; Temmyo, J. Nonpolar (11$\bar{2}$0) p-Type Nirogen-Doped ZnO by Remote-Plasma-Enhanced Metalorganic Chemical Vapor Deposition. *Jpn. J. Appl. Phys.* **2007**, *46* (6L), L549.
(20) Chauveau, J.-M.; Teisseire, M.; Kim-Chauveau, H.; Deparis, C.; Morhain, C.; Vinter, B. Benefits of Homoepitaxy on the Properties of Nonpolar (Zn,Mg)O/ZnO Quantum Wells on a-Plane ZnO Substrates. *Appl. Phys. Lett.* **2010**, *97* (8), No. 081903.
(21) Kozuka, Y.; Tsukazaki, A.; Kawasaki, M. Challenges and Opportunities of ZnO-Related Single Crystalline Heterostructures. *Appl. Phys. Rev.* **2014**, *1* (1), No. 011303.
(22) Taïnoff, D.; Al-Khalfioui, M.; Deparis, C.; Vinter, B.; Teisseire, M.; Morhain, C.; Chauveau, J.-M. Residual and Nitrogen Doping of Homoepitaxial Nonpolar M-Plane ZnO Films Grown by Molecular Beam Epitaxy. *Appl. Phys. Lett.* **2011**, *98* (13), No. 131915.
(23) Temahuki, N.; Jomard, F.; Lusson, A.; Stenger, I.; Hassani, S.; Chevallier, J.; Chauveau, J. M.; Morhain, C.; Barjon, J. Identification by Deuterium Diffusion of a Nitrogen-Related Deep Donor Preventing the p-Type Doping of ZnO. *Appl. Phys. Lett.* **2021**, *118* (10), No. 102106.
(24) Huang, Y.; Li, Y.; Wu, M.; Wang, H. Q.; Yuan, X.; Gholam, T.; Zeng, H.; Wang, J. O.; Wu, R.; Qian, H. J.; Zhang, Y.; Kang, J. Electronic Structure Variations of Polar and Nonpolar ZnO Lattices with Nitrogen-Ion Bombardment Using Synchrotron-Based in Situ Photoemission and X-Ray Absorption Spectroscopy. *J. Synchrotron. Radiat.* **2020**, *27*, 83−89.
(25) Blum, M.; Weinhardt, L.; Fuchs, O.; Bär, M.; Zhang, Y.; Weigand, M.; Krause, S.; Pookpanratana, S.; Hofmann, T.; Yang, W.; Denlinger, J. D.; Umbach, E.; Heske, C. Solid and Liquid Spectroscopic Analysis (SALSA)−a Soft x-Ray Spectroscopy End-station with a Novel Flow-through Liquid Cell. *Rev. Sci. Instrum.* **2009**, *80* (12), No. 123102.
(26) Fuchs, O.; Weinhardt, L.; Blum, M.; Weigand, M.; Umbach, E.; Bär, M.; Heske, C.; Denlinger, J.; Chuang, Y.-D.; McKinney, W.; Hussain, Z.; Gullikson, E.; Jones, M.; Batson, P.; Nelles, B.; Follath, R. High-Resolution, High-Transmission Soft x-Ray Spectrometer for the Study of Biological Samples. *Rev. Sci. Instrum.* **2009**, *80* (6), No. 063103.
(27) Diebold, U.; Koplitzb, L. V.; Duluba, O. Atomic-scale properties of low-index ZnO surfaces. *Appl. Surf. Sci.* **2008**, *237*, 336−342.
(28) Wander, A.; Schedin, F.; Steadman, P.; Norris, A.; McGrath, R.; Turner, T. S.; Thornton, G.; Harrison, N. M. Stability of Polar Oxide Surfaces. *Phys. Rev. Lett.* **2001**, *86*, 3811−3814.
(29) Zhou, H.; Wu, L.; Wang, H.-Q.; Zheng, J.-C.; Zhang, L.; Kisslinger, K.; Li, Y.; Wang, Z.; Cheng, H.; Ke, S.; Li, Y.; Kang, J.; Zhu, Y. Interfaces between Hexagonal and Cubic Oxides and Their Structure Alternatives. *Nat. Commun.* **2017**, *8* (1), No. 1474.
(30) Hu, J.; Guo, W.-P.; Shi, X.-R.; Li, B.-R.; Wang, J. G. Copper Deposition and Growth over ZnO Nonpolar (10$\bar{1}$0) and (11$\bar{2}$0) Surfaces: A Density Functional Theory Study. *J. Phys. Chem. C* **2009**, *113*, 7227−7235.
(31) Patterson, M. C.; Nie, X. W.; Wang, F.; L Kurtz, R.; B Sinnott, S.; Asthagiri, A.; T Sprunger, P. Growth and Structure of Cu and Au on the Nonpolar ZnO (10$\bar{1}$0) Surface: STM, XPS, and DFT Studies. *J. Phys. Chem. C* **2013**, *117*, 18386−18397.
(32) Matsui, H.; Tabata, H. Correlation of Self-Organized Surface Nanostructures and Anisotropic Electron Transport in Nonpolar ZnO (10$\bar{1}$0) Homoepitaxy. *J. Appl. Phys.* **2006**, *99* (12), No. 124307.
(33) Hitchcock, A. P.; Mancini, D. C. Gas phase Core Excitation Spectra Database McMaster University, 2025 http://unicorn.mcmaster.ca/corex/cedb-title.html.
(34) Gejo, T.; Takata, Y.; Hatsui, T.; Nagasono, M.; Oji, H.; Kosugi, N.; Shigemasa, E. Angle-Resolved Photoion Spectroscopy of NO_2 and SO_2. *Chem. Phys.* **2003**, *289* (1), 15−29.
(35) Wight, G. R.; Brion, C. E. K-Shell Energy Loss Spectra of 2.5 keV Electrons in CO_2 and N_2O. *J. Electron Spectrosc. Relat. Phenom.* **1974**, *3* (3), 191−205.
(36) Liu, L.; Xu, J.; Wang, D.; Jiang, M.; Wang, S.; Li, B.; Zhang, Z.; Zhao, D.; Shan, C.-X.; Yao, B.; Shen, D. Z. *p*-Type Conductivity in N-Doped ZnO: The Role of the N_{Zn}−V_O Complex. *Phys. Rev. Lett.* **2012**, *108* (21), No. 215501.
(37) Petravic, M.; Deenapanray, P. N. K.; Coleman, V. A.; Jagadish, C.; Kim, K.-J.; Kim, B.; Koike, K.; Sasa, S.; Inoue, M.; Yano, M. Chemical States of Nitrogen in ZnO Studied by Near-Edge X-Ray Absorption Fine Structure and Core-Level Photoemission Spectroscopies. *Surf. Sci.* **2006**, *600* (7), L81−L85.
(38) Wang, L. G.; Zunger, A. Cluster-Doping Approach for Wide-Gap Semiconductors: The Case of *p*-Type ZnO. *Phys. Rev. Lett.* **2003**, *90* (25), No. 256401.
(39) Yan, Y.; Zhang, S. B.; Pantelides, S. T. Control of Doping by Impurity Chemical Potentials: Predictions for *p*-Type ZnO. *Phys. Rev. Lett.* **2001**, *86* (25), 5723−5726.
(40) Wang, P.; Gong, S.; Li, Y.; Mo, Y. Bond Dissociation Energy of N_2 Measured by State-to-State Resolved Threshold Fragment Yield Spectra. *J. Chem. Phys.* **2024**, *160* (1), No. 014304.
(41) Nakahara, K.; Akasaka, S.; Yuji, H.; Tamura, K.; Fujii, T.; Nishimoto, Y.; Nishimoto, Y.; Takamizu, D.; Takamizu, D.; Sasaki, A.; Sasaki, A.; Tanabe, T.; Tanabe, T.; Takasu, H.; Takasu, H.; Amaike, H.; Amaike, H.; Onuma, T.; Onuma, T.; Chichibu, S. F.; Chichibu, S. F.; Tsukazaki, A.; Tsukazaki, A.; Ohtomo, A.; Ohtomo, A.; Kawasaki, M. Nitrogen doped $Mg_xZn_{1-x}O$/ZnO single heterostructure ultraviolet light-emitting diodes on ZnO substrates. *Appl. Phys. Lett.* **2010**, *97*, No. 013501.
(42) Nugraha; Saputro, A. G.; Agusta, M. K.; Yuliarto, B.; Dipojono, H. K.; Rusydi, F.; Maezono, R. Selectivity of CO and NO Adsorption on ZnO (0002) Surfaces: A DFT Investigation. *Appl. Surf. Sci.* **2017**, *410*, 373−382.
(43) Nugraha; Saputro, A. G.; Agusta, M. K.; Yuliarto, B.; Dipojono, H. K.; Maezono, R. Density Functional Study of Adsorptions of CO_2, NO_2 and SO_2 Molecules on Zn(0002) Surfaces. *J. Phys.: Conf. Ser.* **2016**, *739* (1), No. 012080.
(44) Breedon, M.; Spencer, M. J. S.; Yarovsky, I. Adsorption of NO and NO_2 on the ZnO(2$\bar{1}\bar{1}$0) Surface: A DFT Study. *Surf. Sci.* **2009**, *603* (24), 3389−3399.

https://doi.org/10.1021/acsomega.5c02932
ACS Omega 2025, 10, 39639−39648

(45) Park, C. H.; Zhang, S. B.; Wei, S.-H. Origin of P-Type Doping Difficulty in ZnO: The Impurity Perspective. *Phys. Rev. B* **2002**, *66* (7), No. 073202.

https://doi.org/10.1021/acsomega.5c02932
ACS Omega 2025, 10, 39639−39648